energies

MDPI

Article

Direct Numerical Simulations of Turbulent Flow over Low-Pressure Turbine Blades with Aeroelastic Vibrations and Inflow Wakes

Mahdi Erfanian Nakhchi *, Shine Win Naung and Mohammad Rahmati

Faculty of Engineering and Environment, Northumbria University, Newcastle Upon Tyne NE1 8ST, UK
* Correspondence: mahdi.nakhchi@northumbria.ac.uk

Abstract: In the present work, direct numerical simulation is employed to investigate the unsteady flow characteristics and energy performance of low-pressure turbines (LPT) by considering the blades aeroelastic vibrations and inflow wakes. The effects of inflow disturbance ($0 < \varphi < 0.91$) and reduced blade vibration ($0 < f < 250$ Hz) on the turbulent flow behavior of LPTs are investigated for the first time. The transient governing equations on the vibrating blades are modelled by the high-order spectral/hp element method. The results revealed that by increasing the inflow disturbances, the separated bubbles tend to shrink, which has a noticeable influence on the pressure in the downstream region. The maximum wake loss value is reduced by 16.4% by increasing the φ from 0.31 to 0.91. The flow separation is majorly affected by inflow wakes and blade vibrations. The results revealed that the maximum pressure coefficient in the separated flow region of the vibrating blade has been increased by 108% by raising φ from 0 to 0.91. The blade vibration further intensifies the vortex generation process, adding more energy to the flow and the downstream vortex shedding. The vortex generation and shedding are intensified on the vibrating blade compared to the non-vibrating one that is subject to inflow wakes. The results and findings from this paper are also useful for the design and modeling of turbine blades that are prone to aeroelastic instabilities, such as large offshore wind turbine blades.

Keywords: direct numerical simulation; blade aeroelasticity; fluid-structure interaction; incoming wakes; turbulence modelling

Citation: Erfanian Nakhchi, M.; Win Naung, S.; Rahmati, M. Direct Numerical Simulations of Turbulent Flow over Low-Pressure Turbine Blades with Aeroelastic Vibrations and Inflow Wakes. *Energies* **2023**, *16*, 2803. https://doi.org/10.3390/en16062803

Academic Editor: Giuseppe Pascazio

Received: 1 February 2023
Revised: 6 March 2023
Accepted: 7 March 2023
Published: 17 March 2023

1. Introduction

Low-Pressure Turbines (LPTs) are an important component of gas turbine engines used to power passenger aircraft. The engine thrust is mainly generated by a fan driven by an LPT, which weighs up to 30% of the overall engine weight [1]. LPTs are also an important part of the gas turbines used to run electric power generators. The efficiency and structural integrity of an LPT are effectively influenced by the aerodynamic and aeroelastic behavior of the turbine blades under the influence of flow disturbances [2]. Therefore, the realistic prediction of the aerodynamics and aeroelasticity of LPTs by using numerical methods has become popular among many researchers.

Though the aerodynamic flow structure over turbine rotor blades is three-dimensional and unsteady turbulent, only a few studies have focused on low-pressure gas turbine blades because of practical limitations [3]. It is possible to reduce the weight of LPTs by designing relatively thinner high-lift blades. Therefore, the aeroelasticity and structural integrity of the blades need to be examined carefully. However, the interactions of various sources of flow disturbances and their influences on blade aeroelasticity are not well understood. The flow separation over LPTs will cause the transition to turbulence and vortex generation in the downstream region of the blades. Kubacki et al. [4] used the Reynolds Average Navier-Stokes (RANS) method to investigate the flow structure over a stationary T106A LPT blade with clean inflow conditions. They investigated the pressure coefficient and

velocity profiles in the laminar to turbulent flow transition period. Han et al. [5] used the RANS method with the SST turbulent model to investigate the aerodynamic performance of high-pressure and low-pressure axial turbines. They investigated the pressure coefficient variations at the middle blade section of LP turbine blades. Marty [6] used both RANS and Large Eddy Simulation (LES) methods to analyze the laminar separation bubble (LSB) on the surface of the T106C LPT blade. They found that the LES model can better predict the LSB formation flow instabilities compared to the RANS method because of the transitional flow regime. Rahmati et al. [7,8] developed nonlinear time and frequency domain techniques to investigate the aeroelasticity and unsteady aerodynamics of low-pressure turbines and multirow compressors of gas turbine engines. Their results show that the inflow disturbances or flow reflection from adjacent blade rows can significantly affect the aeroelastic behaviours of turbomachinery blades.

Flexible blades and vibrations have a noticeable influence on the performance of turbines [9]. Investigation of fluid-structure interaction among the blades and the air flow needs high-fidelity numerical simulations [10,11]. Win Naung et al. [12] numerically investigated the impacts of vibrations on the vortex production and wake behavior of an LPT blade. They also implemented a harmonic balance method in their simulations and concluded that five harmonics are required to compare their results with the time domain solution method. They also found that the blade vibrations have a strong effect on the wake profile and flow disturbance in the downstream region of the LPT blades. Fan et al. [13] numerically studied the effects of vortex-induced vibration on vorticity generation on two immersed cylinders with short spans. They proposed a nonlinear aerodynamic damping coefficient into their simulations and concluded that the proposed model only works for high Scruton numbers and cannot predict flow structure and vorticity fluctuations due to vibrations. Wang and Zou [14] performed a numerical study to investigate the effects of geometrical parameters on the performance of turbine blades. They used PC-Kriging for the uncertainty analysis together with the RANS solver to investigate the effects of the design parameters on the boundary-layer shape factor (H), the total pressure loss (L_c), and other aerodynamic characteristics of the turbine blades. They concluded that the incoming wake has a significant influence on flow behavior and vortex generation on gas turbine blades.

Zhang et al. [15] predicted the time-averaged wake of wind turbines by using convolutional neural networks (CNN). They compared their numerical results with the CNN method and found that their proposed model is computationally more efficient to predict the wake compared the numerical analysis. Qu et al. [16] used the RANS method to investigate the turbulent flow structure and secondary flows over high-pressure turbine blades by considering the periodic wake effects. They suggested that the contoured end wall with a wake decreased secondary kinetic energy by 53.8%. But, as argued by Tucker [17], RANS/URANS methods cannot correctly evaluate the transient flow structure and flow instabilities, especially in the separated region, which can be commonly observed in LPTs. Therefore, performing high-fidelity numerical simulations can help designers examine the effects of vorticities and flow disturbances on the LPT blades in gas turbines.

High-fidelity methods such as LES or Direct Numerical Simulations (DNS) could be more accurate, and instantaneous physical details of turbulent flows can be detected [18]. Wang et al. [19] used LES to numerically study the transitional flow separation on an LP turbine. Siddiqui et al. [20] developed a finite-volume high-fidelity method linked with the reduced-order finite element method of incompressible flows. Jia et al. [21] performed LES over low-pressure turbine blades to investigate the separating point on the turbine blades. They concluded that at low Mach numbers, the proposed method is not efficient. Zaki et al. [22] conducted a DNS study investigating the flow structure over stationary compressor blades. They also computed the boundary layer structure over the surface of the blade, and the results agree well with the experimental data. Wheeler et al. [23] performed DNS on high-pressure turbines and examined the physical characteristics of the transient fluid structure. Moriguchi et al. [24] used the LES method to investigate the effects of trailing edge (TE) cutback on the flow structure and vortex generation over the surface of

the linear turbine blade. They concluded that the TE cutback has a considerable influence on the boundary layer thickness and the pressure coefficient. They also investigated the breakdown loss due to the variations in the TE shape. Most recently, Lyer et al. [25] used high-order DNS to investigate the flow over the MTU-T161 low-pressure turbine blade. They used a Python-based solver, named PyFR, to run the simulations for the Reynolds number of 200,000. It was concluded that the proposed DNS method can capture more mode details of the flow separation compared to typical RANS methods. Wei et al. [26] performed LES over T106 low-pressure turbine blades. They concluded that due to the huge CPU time requirement for 3D simulations, they only used 5% of the chord length for their simulations, which is not enough to capture all the details of the realistic airflow behaviour. To accurately capture the three-dimensional vorticities in the separated region, it is necessary to conduct a full 3D analysis on a low-pressure turbine blade. The main disadvantage of these LES and DNS methods is the huge amount of computational resources required, which can even surpass the capacity of supercomputers. In addition, it is impractical to consider all complex and realistic physical conditions in multi-stage turbines, such as the aeroelastic oscillations and inflow wakes. However, these parameters have considerable effect on flow separation in LP turbines, which have not been considered in any previous DNS studies.

The spectral-hp element method is a powerful numerical technique with high accuracy that is used to analyze the aerodynamic performance of turbomachinery [27]. This DNS method is based on finite element and spectral techniques [28]. One main advantage of this method is that it requires much fewer computational resources compared to other high-fidelity DNS methods. This method can be employed to calculate the flutter instabilities over the gas turbine blades by considering the forced vibrations or vortex-induced vibrations (VIV) of the blades. The effects of aeroelastic vibrations can be included by using a moving reference frame. Bao et al. [29] utilized the spectral-hp element method to explore the effects of vortex-induced vibrations on the pressure coefficient and recirculation flows over a flexible riser. In another DNS study, Cassinelli et al. [30] applied the spectral-hp element technique to numerically analyze transitional flow behavior, boundary-layer velocity, and turbulent kinetic energy over the surface of an LP turbine blade without considering the blade vibrations. This method has also been used to investigate the transitional flow regime over various aerodynamic structures with incompressible or compressible flow conditions [31,32].

According to a literature review, a precise estimate of flow characteristics and separation over the LP turbine blades is critical in the design of aircraft engines. However, most previous studies used RANS methods to investigate the turbulent flow characteristics on the surface of LPTs. However, the flow structure over the turbine blades is transient, and it is essential to predict and capture the flow instability on the blades by using a DNS method. In the present paper, the spectral-hp element method has been used to predict the details of the transitional flow structure and pressure coefficient over the LPT blades by consideration of the simultaneous effects of inflow wakes and blade vibrations on the flow structure of LPT blades. In summary, the main novelties of the present work can be expressed as follows:

- To develop a highly accurate DNS method to investigate the flow structure, wall shear stress, pressure coefficient, instantaneous vortex generation, flow separation, and other essential parameters in the design of LPT blades.
- For the first time, the effects of aeroelastic vibrations and inflow wakes are considered simultaneously in a DNS study on gas turbine engines.

The novel proposed model can help the designers to improve the efficiency of the gas turbines and aircraft engines by capturing the details of flow fields and its effects on aerodynamics and the aeroelasticity of LPTs.

2. Physical Model

Figure 1 displays the schematic of the oscillating T106 blades in the LP turbine cascade. The blades vibrate with a specific vibration frequency (f = 250 Hz) and amplitude ($0 < A < 3\%$ chord) in the normal direction. For validation purposes and to compare the aerodynamic performance of non-oscillating T106 blades, the flow conditions used in this study is the same as those used by Wei et al. [26]. The span length (L) is assumed to be 0.4C. The Reynolds number is defined as $Re = \frac{UC}{\nu}$. The DNS investigations of the T106 blade are made at the Reynolds number of 51,800 to investigate the effects of various realistic flow conditions on instantaneous flow structure and flow separation on the blades. Various inflow conditions (clean inflow and incoming wakes with three different frequencies) are investigated in this study. To generate the inflow disturbance (φ), the same method of Michelassi et al. [33] is used in the present DNS study. Moving cylindrical rods with a diameter of 0.02C are implemented in the upstream region of the leading edge of the LP turbine blade. The cylinders have a velocity of $u_{bar} = -0.41\ U$ in the y-direction. The flow disturbance φ is defined by $\varphi = \mathrm{F.C/V_{2is}}$ where f and $\mathrm{V_{2is}}$ are the passing frequency and isentropic exit velocity, respectively. By changing the bar spacing, different dimensionless inflow disturbances $(\varphi = 0.0, 0.31, 0.61, 0.91)$ can be achieved, in which $\varphi = 0$ represents the clean inflow boundary condition. The values of the inflow disturbance are selected based on the study of Michelassi et al. [33] for validation and comparing purposes.

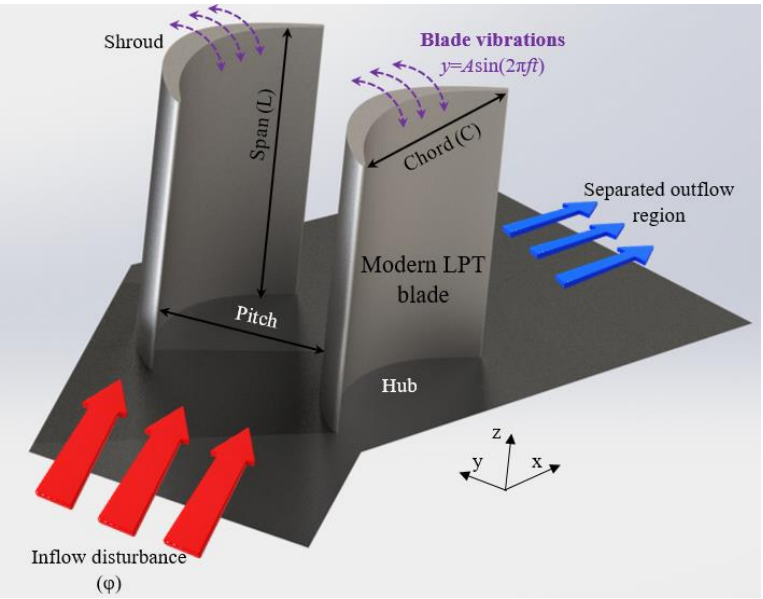

Figure 1. Schematic of the T106 low-pressure turbine with the geometrical parameters.

The details of the forces on the T106 blade are provided in Figure 2. The geometrical definitions of T106 blade are given in Table 1. The blades are fixed at the hub with aeroelastic harmonic oscillations of $y = A\sin(2\pi ft)$ at the blade shroud. The pitch-to-chord length ratio (s/C) is selected as 0.798. The non-dimensional chord length (C) is set as one, and the non-dimensional axial chord length (C_{ax}) is selected as 0.85C. The inlet angle of 45.5° is selected for the present numerical simulations, which is in agreement with previous numerical investigations over stationary LP turbine blades. The outlet angle is set at 63.2° with an exit Mach number of 0.59. The geometry details of the T106 blade can be found in [34].

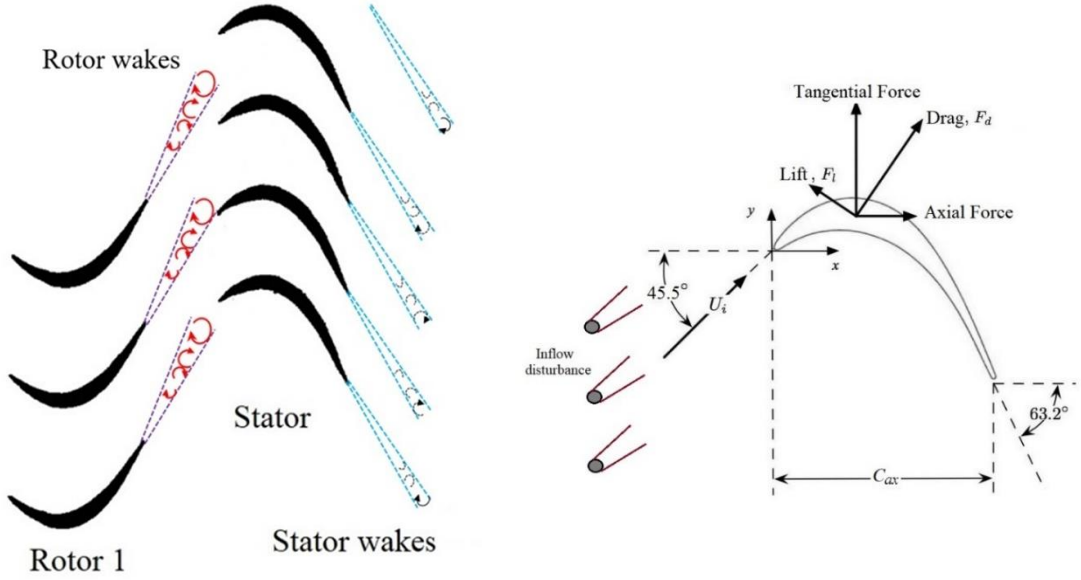

wake structure in a multi-stage LP turbine Detailed view of forces on the blade

Figure 2. Schematic view of the wake generation in a multi-stage turbine and forces over LP turbine blade.

Table 1. Geometrical and physical parameters of the T106 LP turbine cascade.

Parameter	Symbol	Value	Parameter	Symbol	Value
Chord length	C	99 mm	Pitch to chord length	s/C	0.798
Axial chord length	C_{ax}	85 mm	Cylindrical rod diameter	d	$0.02C$
Inflow angle	β_1	37.7°	Cylinder velocity	u_{bar}	$-0.41U$
Exit angle	β_2	63.2°	Reduced vibration frequency	f_{red}	0.51
Trailing edge thickness	-	1.8 mm	Reynolds number	Re	50,000–51,800
Trailing edge radius	-	0.5 mm	Inflow disturbance	φ	0–0.91
Span length	L	$0.8C$			

3. Results

The high-fidelity analyzes with high-order spectral-hp element approach in NEKTAR++ solver are under the following assumptions: (i) constant thermophysical properties of the working fluid; (ii) incompressible turbulent flow; (iii) the flow is unsteady and transient; and (iv) a three-dimensional model. The Navier-Stokes equations in their non-dimensional form can be expressed as:

$$\frac{\partial U_i}{\partial X_i} = 0 \tag{1}$$

$$\frac{\partial U_i}{\partial t} + \frac{\partial}{\partial X_i}(U_i U_j) = -\frac{\partial P}{\partial X_j} + \frac{1}{Re}\nabla^2 U_j \tag{2}$$

where P and Re are pressure and Reynolds number of the working fluid (air). The proposed high-fidelity method could capture the details of the vorticity generation and time-dependent variables of turbulent flow over the surface of the oscillating LP turbine blade with various inflow wakes. The moving reference frame (MRF) scheme is utilized to impose forced vibrations on the surface of the blades.

The spectral-hp element methodology, the Galerkin scheme, has been used to investigate the turbulent flow on the vibrating LP turbine blades. In the methodology, the domain is decomposed into subdomains, such as $\Omega = \bigcup_{e \in \varepsilon} \Omega_e$. Where Ω is the computational domain in the global coordinate system. The solver converts the geometry from the local geometry (x_1, x_2) to a reference coordinate system of (ξ_1, ξ_2) as:

$$x_1 = \chi_1^e(\xi_1, \xi_2),\ x_2 = \chi_2^e(\xi_1, \xi_2) \tag{3}$$

The output parameters, such as velocity components $u(\xi_1, \xi_2)$, can also be converted by using the moving reference frame in the spatial domain as [35]:

$$u(\xi_1, \xi_2) = \sum_{n \in \mathbb{N}} F_n(\xi_1, \xi_2)\hat{u}_n = \sum_{p=0}^{P} \sum_{q=0}^{P} \varphi_p(\xi_1)\varphi_q(\xi_2)\hat{u}_{pq} \tag{4}$$

The momentum equation can be written as:

$$\frac{\partial U_i}{\partial t} = N(\mathbf{u}) - \nabla p + \frac{1}{Re}\mathcal{L}(\mathbf{u}) \tag{5}$$

In Equation (5), $N(\mathbf{u}) = \frac{\partial}{\partial X_i}(U_i U_j)$ and $\mathcal{L}(\mathbf{u}) = \nabla^2 U_j$ are the convective and diffusive terms of the momentum equation, respectively. Based on the velocity-correction scheme (VCS) and the advection, Poisson and Helmholtz terms can be written as:

$$u^* = -\sum_{m=1}^{J} \alpha_m u^{n-m} - \Delta t \sum_{m=0}^{J-1} \beta_m N\left(u^{n-m}\right) \tag{6}$$

$$\nabla^2 p^{n+1} = \frac{1}{\Delta t}\nabla.\mathbf{u}^* \tag{7}$$

$$\nabla^2 \mathbf{u}^{n+1} - \frac{\alpha_0}{\nu \Delta t}\mathbf{u}^{n+1} = -\frac{\mathbf{u}^*}{\nu \Delta t} + \frac{1}{\nu}\nabla p^{n+1} \tag{8}$$

where $^{n+1}$th time step after performing integration over time and using Equations (6)–(8) can be discretized as [36]:

$$\frac{\sigma_0 \mathbf{u}^{n+1} - \sum_{m=0}^{J_i-1} \alpha_m \mathbf{u}^{n-m}}{\Delta t} = \sum_{m=0}^{J_e-1} \beta_m N\left(\mathbf{u}^{n-m}\right) - \nabla p^{n+1} + \frac{1}{Re}\mathcal{L}(\mathbf{u}^{n+1}) \tag{9}$$

This equation could be simplified as:

$$\frac{\sigma_0 \mathbf{u}^{n+1} - \mathbf{u}^*}{\Delta t} = N^+ - \nabla p^{n+1} + \nu \mathcal{L}(\mathbf{u}^{n+1}) \tag{10}$$

where $\mathbf{u}^* = \sum_{m=0}^{J_i-1} \alpha_m \mathbf{u}^{n-m}$ and $N^+ = \sum_{m=0}^{J_e-1} \beta_m N(\mathbf{u}^{n-m})$ are the series of decomposed terms. By integrating over the computational domain Ω, the Poisson equation can be written as:

$$\int_\Omega \nabla p^{n+1}.\nabla \aleph d\Omega = \int_\Omega \left[\frac{\mathbf{u}^* - \sigma_0 \overset{\sim}{\mathbf{u}}^{n+1}}{\Delta t} + N^+ - \frac{1}{Re}(\nabla \times \nabla \times \mathbf{u})\right].\nabla \phi d\Omega \tag{11}$$

where $\nabla \aleph$ is the operational function in the domain Ω. Finally, $\mathbf{u}$ can be computed as [28]:

$$u^\delta(\xi, t) = \sum_i \hat{u}_i \aleph_i(\xi, t) \tag{12}$$

A precise high-order outflow boundary condition, which is a popular model in unbounded physical domains, is employed in the present DNS study over the LP turbine

blades with inflow wakes. The equation below is utilized to treat the outflow boundary condition [37]:

$$p^{n+1} = \nu \mathbf{n}.\nabla.\mathbf{u}^{*,n+1}.\mathbf{n} - \frac{1}{2}\left|\mathbf{u}^{*,n+1}\right|^2 S_0\left(\mathbf{n}.\mathbf{u}^{*,n+1}\right) + f_b^{n+1}.\mathbf{n} \quad (13)$$

where $S_0(n.\mathbf{u}) = \frac{1}{2}(1 - \tanh\frac{n.\mathbf{u}}{u_0\delta})$ is a scalar function, $\mathbf{u}_0$ denotes the characteristics of velocity, and $\delta > 0$ is a small dimensionless constant. The convergency can be controlled by a spectral vanishing viscosity (SVV). SVV Cutoff Ratio = 0.5 and SVV Diff Coefficient = 0.1 are used to avoid divergence of the simulations. The DG-kernel methodology is used for the SVV coefficient. By increasing the polynomial order (P), the Courant–Friedrich–Lewy (CFL) number becomes larger, and therefore, the time step should be reduced. The simulations were performed with a time step of $\Delta t = 10^{-4}$ sec when p = 5, and it was decreased to $\Delta t = 2 \times 10^{-5}$ sec when p = 9 to make sure that the CFL number remained less than one. The open-source NEKTAR++ code (v 5.2.0) is employed on the national supercomputer of the UK (ARCHER-2) with different numbers of AMD 2.2 GHz CPU cores (128 cores for lower polynomial orders and 512 cores for high-order simulations) and an allocated 256 GB of memory.

This section may be divided by subheadings. It should provide a concise and precise description of the experimental results, their interpretation, as well as the experimental conclusions that can be drawn.

3.1. Mesh Generation

Figure 3 depicts the details of the computational domain and grid generation in the linear low-pressure turbine cascade of T106 blades. However, the polynomial order used for the final simulations must be selected based on a grid independence study to properly capture the instantaneous variations of the vorticity production on the oscillating turbine blade with inflow wakes (discussed in the next section). Twelve inflation boundary-layer prism meshes with the smallest layer size of 0.002 m for the layer close to the blade wall and a growing ratio of 1.15 have been selected to resolve the laminar viscous sub-layer resolution. The mesh size in the downstream region of the blade and also in the inflow disturbance region is smaller than the other regions to precisely detect the transient flow details due to the aeroelastic vibrations of the blades.

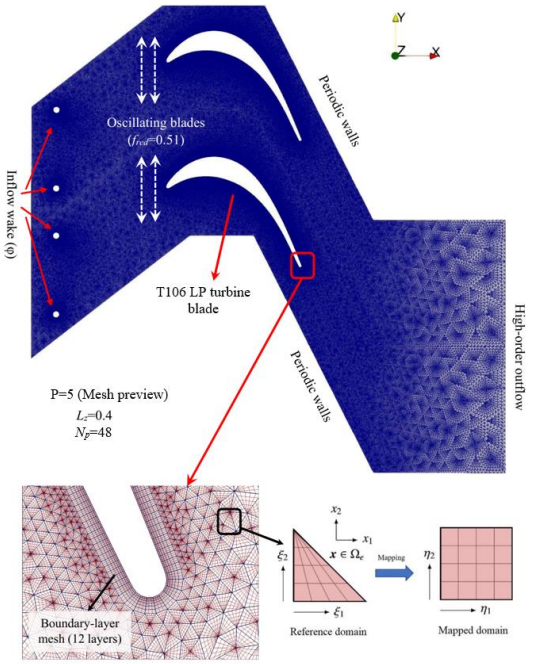

Figure 3. Mesh generation in the computation domain of T106 blade with p = 5.

A grid study is performed on the number of Fourier layers in the span direction. By comparing the results of different numbers of layers, ranging from 24 to 64 layers, it was observed that N_p = 48 layers provided the most accurate results. Using a higher number of layers than 48 will increase the computation cost without impacting the flow characteristics. As discussed earlier, each element will be decomposed from the original domain into the mapped domain through a mapping function. The details of the mapping process are also shown below.

3.2. Viscous Sub-Layer Resolution

Before performing further DNS simulations according to the spectral-hp element method, the most appropriate polynomial order must be investigated. To find the most accurate P-order for an accurate prediction of the unsteady flow behavior over the surface of the oscillating LP turbine blade and detect realistic fluctuations of the pressure and vortex generation, a different analysis was conducted for the grids ranging from p = 5 to 11. It was observed that p = 9 is the most accurate polynomial order and the pressure coefficient variations on the suction side of the oscillating T106 blade with various inflow wakes will be less than 0.5% compared to a higher polynomial order of 11. Therefore, it is selected for the DNS simulations.

The boundary layer grid with 12 inflated layers is selected for the DNS study to resolve the viscous sub-layer effects and to accurately predict the causes of aeroelastic vibrations on the flow structure on the suction side of the blades. To make sure the wall+ parameters are in an appropriate range, the following condition should be met: $\Delta n^+ < 1$ [38]. During entire simulations, the normalised grid size in the streamwise (Δs^+), and spanwise direction (Δz^+) are also kept less than 10 [38]. The wall+ values over the surface of the vibrating T106 blade with clean inflow (φ = 0) are shown in Figure 4. The wall+ values are all within acceptable ranges. Consequently, the prism mesh is accurate enough to capture the flow structure and flow separation in the boundary layer region of the oscillating T106 low-pressure turbine.

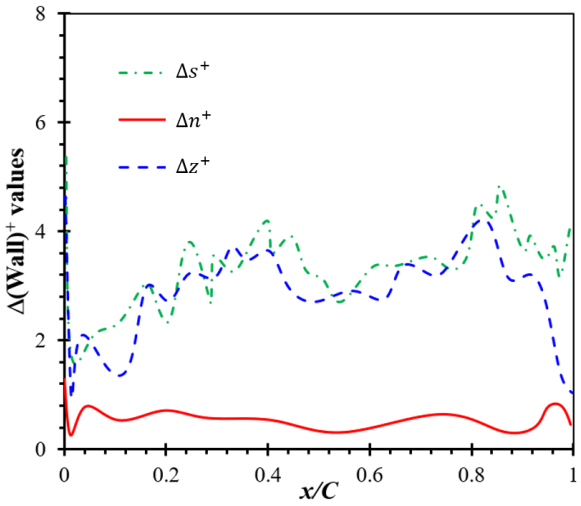

Figure 4. Instantaneous wall$^+$ values on the surface of the vibrating T106 low-pressure turbine blade for φ = 0, f_{red} = 0.5, A = 1%.

4. Results and Discussion

Validation

Prior to investigating the impact of the inflow disturbances on the unsteady flow behavior, the DNS simulation based on a stationary blade without any inflow wakes is first made for validation of the numerical model. The wake deficit profile Ω is specified as $(p_{t\text{-}in} - p_t)/(p_{t\text{-}in} - p_{rf})$, in which p_t is the total pressure and p_{rf}, and $p_{t\text{-}in}$ are the reference pressure and the total inlet pressure, respectively. The wake deficit is obtained at 40% of

the chord length downstream of the trailing edge of the blade. Ω predicted by the present DNS simulation is compared to those of the experiment [39] and the reference simulation using an unsteady finite volume method [12], and they are presented in Figure 5. Overall, a close agreement is achieved between the present DNS simulation and the experimental data. Likewise, the pressure coefficient C_p from the present simulation is compared to the experiment and the reference simulation using a finite volume method [12], as shown in Figure 5. C_p is calculated as $(p_w - p_{rf})/(p_{t\text{-}in} - p_{rf})$, where p_w is the surface pressure. It is seen that the C_p distribution predicted by the present simulation is in very good agreement with the experiment and the reference simulation. The obtained results are also in good agreement with the numerical results of Nakhchi et al. [40] over stationary low-pressure turbine blades with clean inflow conditions. Therefore, it is deduced that the method reasonably resolves the unsteady flow and the downstream wake, which is considered sufficient for further simulations involving inflow disturbances and blade vibrations.

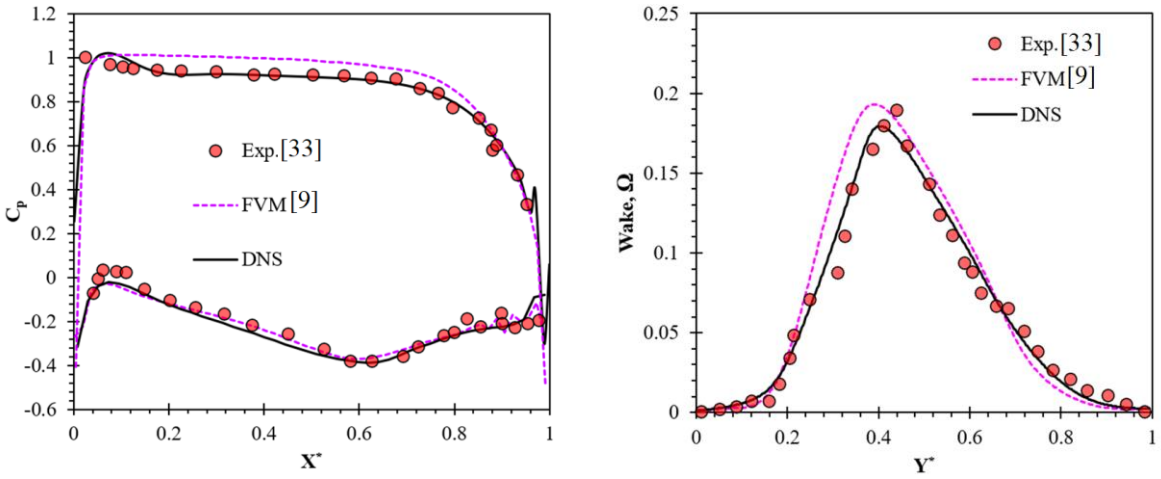

(**a**) Pressure coefficient (**b**) Wake profile

Figure 5. Validation of C_p and wake loss profiles (Ω) with the previous experiments [39] and the numerical data [12] over a non-oscillating T106 blade.

Figure 6 compares the iso-surfaces of vorticity (coloured by velocity) between the stationary and vibrating blade cases with and without inflow wakes to qualitatively highlight the flow structures that occurred due to blade vibration. The inflow wakes at different frequencies, which are achieved by placing a different number of cylinders in the upstream region of the blade. The cases using a stationary blade will be first discussed. When there is no inflow wake present at the inlet, the flow separation occurs near the trailing edge due to the curvature of the blade and the angle of attack of the incoming flow. When there is an inflow wake upstream of the blade, the flow across the blade is extremely distorted. At φ = 0.31, the vortex structures from the wake mostly influence the pressure surface of the blade before contributing to the downstream wake. At φ = 0.61, the suction surface of the blade is more affected by the wake structures, whereas the flow structures travel underneath the pressure surface and hit the trailing edge of the blade, where they combine with those from the pressure surface. However, at φ = 0.91, the T106 blade is influenced by the inflow wake. As a result, the downstream wake is stronger than that of those with a stationary blade. The blade vibration triggers more flow disturbances. It can be clearly observed in the case of a clean inflow without wakes. It is seen that strong vortex structures are generated on the suction side due to the blade motion. These flow structures travel downward and contribute to the vortex shedding, resulting in a larger downstream wake. A combination of inflow wake and blade vibration causes significant flow distortions around the blade, and both pressure and suction surfaces are affected. This leads to high-intensity turbulence and wake in the downstream region. It is very clear in

the case of φ = 0.91 that the downstream wake is not only highly unsteady and turbulent but also dramatically large in size.

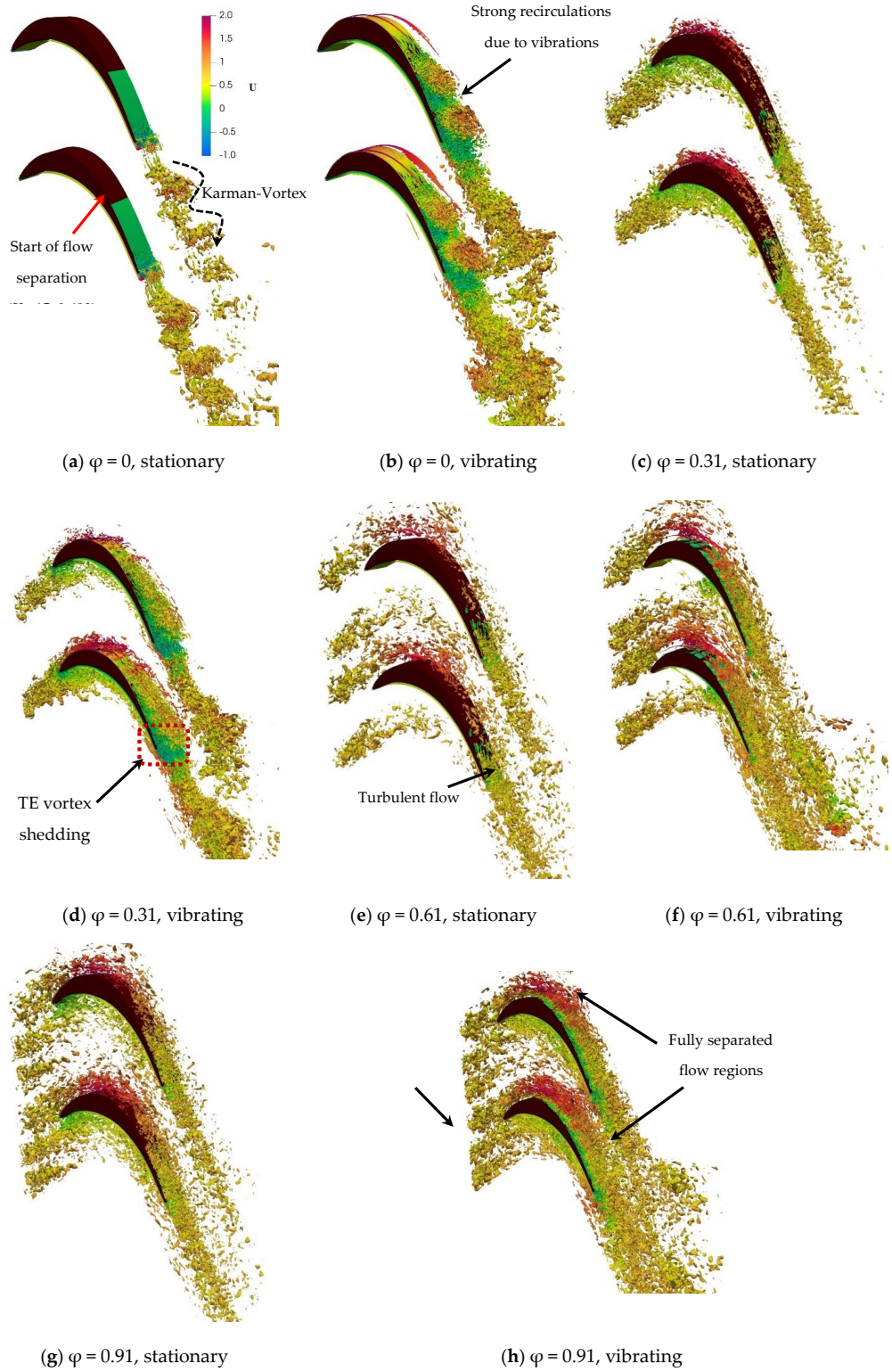

(**a**) φ = 0, stationary (**b**) φ = 0, vibrating (**c**) φ = 0.31, stationary

(**d**) φ = 0.31, vibrating (**e**) φ = 0.61, stationary (**f**) φ = 0.61, vibrating

(**g**) φ = 0.91, stationary (**h**) φ = 0.91, vibrating

Figure 6. The effects of the inflow wakes (φ) and the vibrations on the vorticity contours over the LP turbine blade.

The vortex development near the trailing edge resolved by the present DNS model and those of the experiment [41] and the previous LES model [26] for a stationary blade

subject to no inflow wakes are compared in Figure 7. It is seen that the LES model can reasonably provide the vortex shedding from the trailing edge. However, the method can detect the vorticity production in more detail, and it is comparable to the experiment. In particular, the DNS model resolves and provides detailed vortex structures in the downstream wake region, which are difficult to capture by lower-fidelity models as well as the experiment. Therefore, the use of a DNS model should be considered in the design of low-pressure turbine blades, and the present DNS model is found to be much more efficient at a reasonable computational cost than other typical finite volume DNS models.

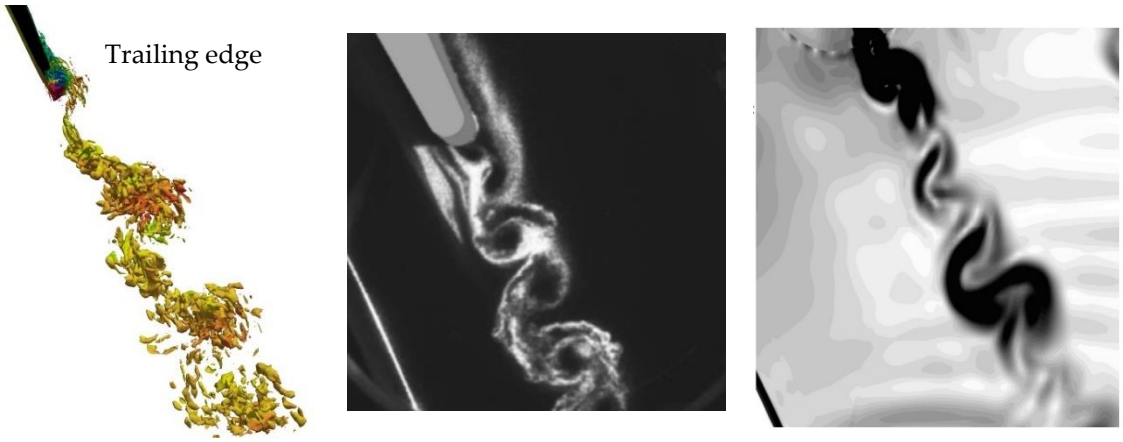

Figure 7. Comparison of the vortex generation near the TE of non-oscillating T106 blade with clean inflow with previous experimental and numerical data for Re = 5×10^5. (**a**) Present DNS study. (**b**) Experimental [41]. (**c**) LES model [26].

To better understand the physical behavior of the turbulent flow subject to incoming wakes and blade vibration, the turbulent kinetic energy contours around the T106A turbine blade are plotted at $\varphi = 0.31$ and 0.91 for both stationary and vibrating blades in Figure 8. At $\varphi = 0.31$, the turbulent flow resulting from the inflow wake decay and the flow distortion occurs in the blade passage. Apart from the area close to the cylinder where the wake is generated, the maximum turbulent kinetic energy is seen in the downstream wake region. In the case of the stationary blade, the maximum value was captured in the region next to the trailing edge. In contrast, it is evident that the blade vibration adds more turbulence to the flow. Subject to the same inflow wake condition, the kinetic energy flow is much higher on the suction surface. Increasing the inflow wake frequency to $\varphi = 0.91$, the turbulent flow is observed around the stationary blade. Similar to the $\varphi = 0.31$ case, the turbulent kinetic energy distribution is intensified by the blade vibration. In particular, the maximum values of the turbulent kinetic energy are observed almost all over the suction surface, in addition to the downstream wake region.

Figure 9 illustrates the wall shear stress distribution for different inflow frequencies. It is found that the blade oscillations have a noticeable influence on the wall shear stress distribution in both clean inflow and inflow wake cases. Compared to the clean inflow case, the inflow wake also has an effect on the wall shear stress, especially near the trailing edge. Besides, the region in close proximity to the leading edge is also affected by the wake at a high frequency. The wall shear stress, depending on its level of intensity, is directly associated with the flow separation and recirculation on the suction side.

The flow streamlines in the blade passage of the T106A turbine are demonstrated in Figure 10. The figure provides the effect of the inflow wake and the blade vibrations on the behavior of the flow. For clean inflow, it is clear, without the effect of the distortion due to the wake, that the flow is affected by the vibrations. The oscillations cause flow separation on the suction surface with some recirculation in the separation zone. Inflow wakes add

further flow disturbances. The streamlines traveling over the pressure surface are more affected by the wake.

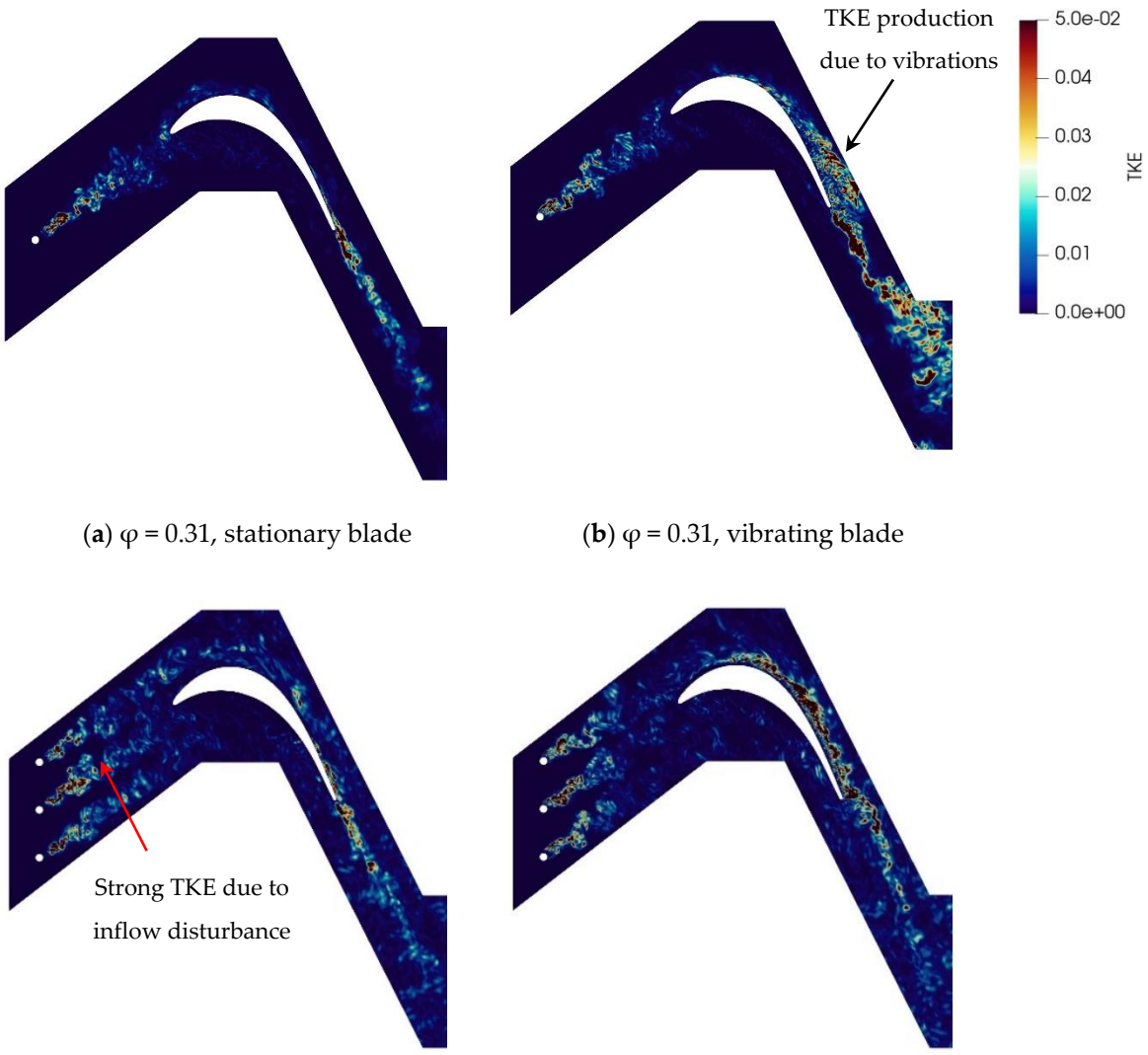

(**a**) φ = 0.31, stationary blade (**b**) φ = 0.31, vibrating blade

(**c**) φ = 0.91, stationary blade (**d**) φ = 0.91, vibrating blade

Figure 8. The effects of the vibrations and the inflow wake on the TKE contours behind the T106 blade.

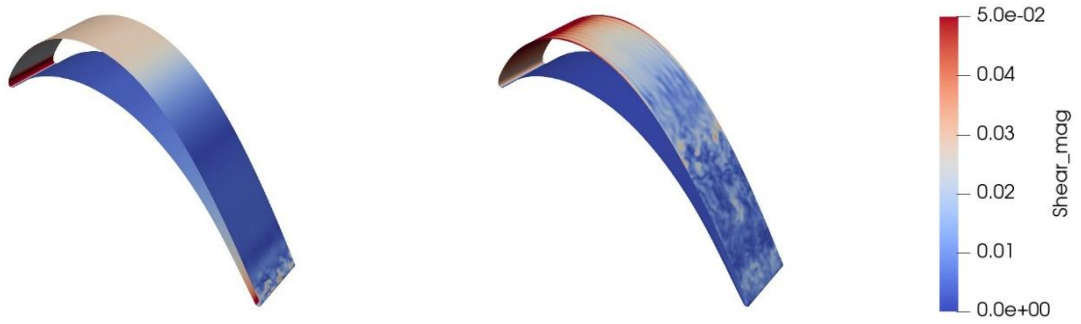

(**a**) φ = 0, stationary blade (**b**) φ = 0, vibrating blade

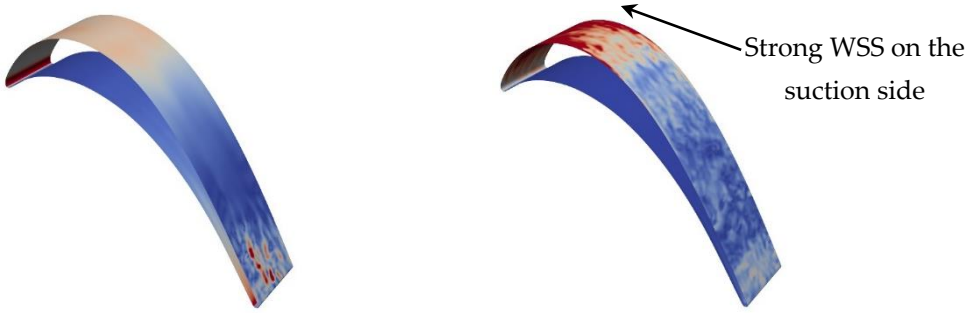

(**c**) φ = 0.31, stationary blade (**d**) φ = 0.31, vibrating blade

(**e**) φ = 0.61, stationary blade (**f**) φ = 0.91, stationary blade

Figure 9. Wall shear stress contours over the non-oscillating and oscillating turbine blades with different inflow disturbance.

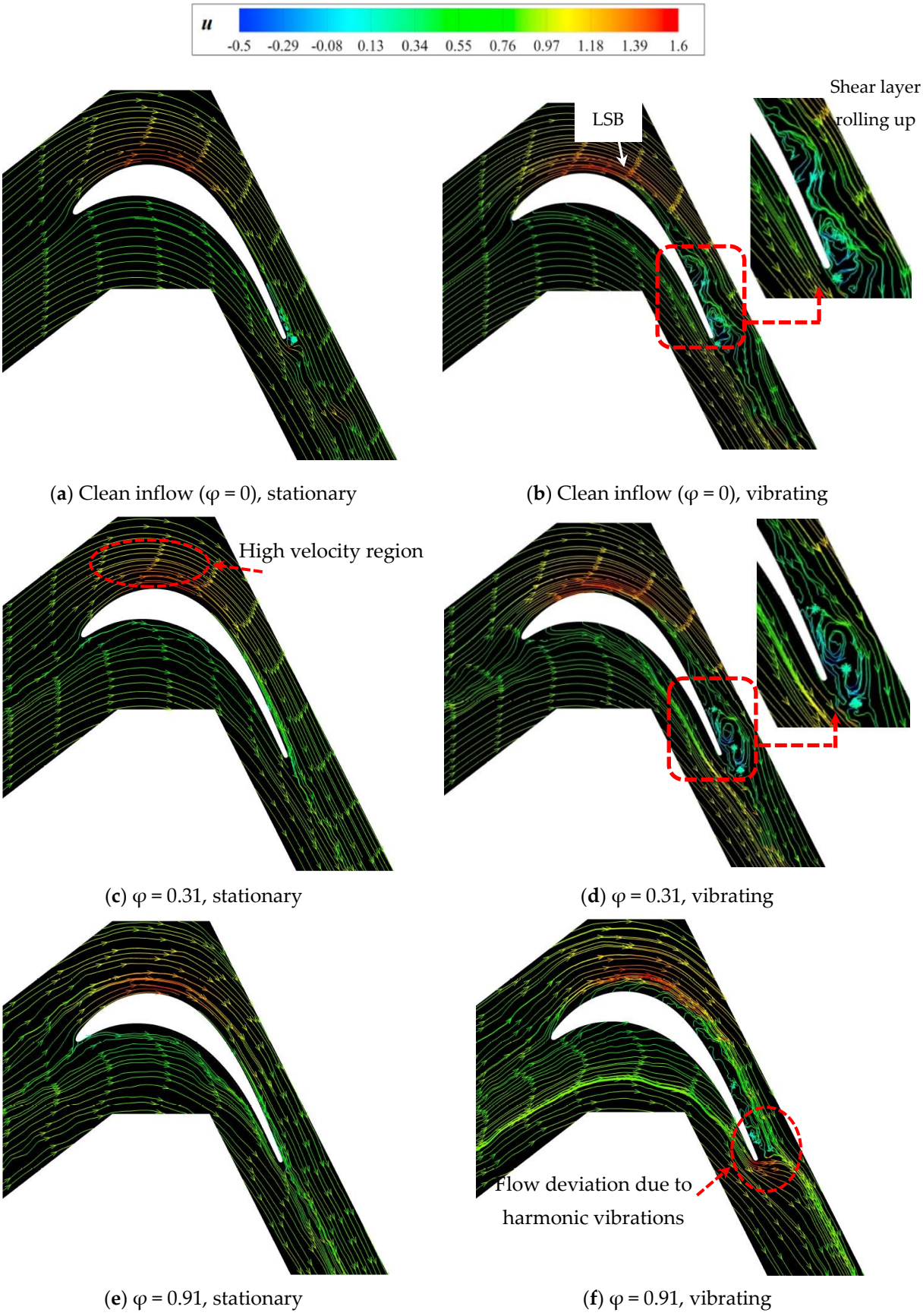

(**a**) Clean inflow (φ = 0), stationary

(**b**) Clean inflow (φ = 0), vibrating

(**c**) φ = 0.31, stationary

(**d**) φ = 0.31, vibrating

(**e**) φ = 0.91, stationary

(**f**) φ = 0.91, vibrating

Figure 10. Effects of the vibrations and the inflow disturbance on the flow streamlines over the blade.

The effect of inflow wakes on the downstream wake profile of the stationary blade case is presented in Figure 11. The wake loss is defined as $(p_{t\text{-}in} - p_t)/(p_{t\text{-}in} - p_{ref})$, where p_t is the total pressure, and measured at 40% of the chord length in the downside region. The dimensionless pitch (Y^*) is defined as Y/Pitch. It is observed that the profile is slightly reduced by increasing the inflow disturbance from $\varphi = 0$ to 0.91. By raising the inflow disturbance, the separated bubbles tend to shrink, which has a noticeable influence on the pressure value in the downstream region. The inflow disturbance reduces the boundary-layer separation region. It is observed that the maximum value occurs at $Y^* = 0.401$, and it moves downward to $Y^* = 0.492$ by raising φ from 0 to 0.91.

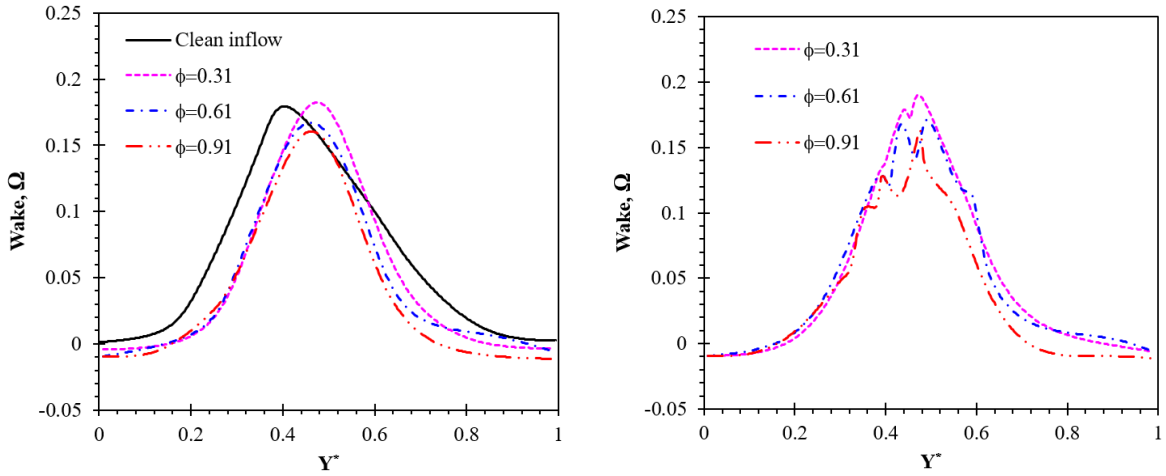

(**a**) Stationary blade (**b**) Oscillating blade

Figure 11. The effects of the inflow wake and the blade vibrations on the wake profile over the low-pressure turbine blade at Re = 5.18×10^4.

It was previously discussed that the downstream vortex shedding is stronger with more vorticity structures in the wake. Moreover, the maximum wake loss value is reduced by 16.4% by increasing the inflow wake (φ) from 0.31 to 0.91. It was also noticeable that the vortex structures are broken into smaller pieces in the wake region due to inflow wakes. These factors contribute to the shift in the peak of the wake profile. Furthermore, it is obvious that the blade oscillations have a great impact on the wake profile. Similar to the rigid (non-oscillating) blade, the profile is reduced as the inflow wake frequency is increased. The peaks of the profiles are also found at $Y^* = 0.501$. Significant deviations in the profile can be seen between $0.3 < Y^* < 0.6$. The blade vibration triggers additional flow disturbances, which add more turbulence to the downstream wake. In addition, the downstream wake is distorted by the blade motion. As a result, the profile is highly affected, and fluctuations are observed in the profiles.

Time-averaged pressure coefficients C_p computed from different inflow conditions over the surface of the vibrating low-pressure T106 turbine blade are shown in Figure 12. By increasing the inflow disturbance parameter from $\varphi = 0$ to 0.91, the separation bubble diminishes and flow reattachment occurs at the upstream region on the suction side, resulting in a pressure coefficient increment in the region of $0 < X^* < 0.6$. This flow behavior was previously shown in Figure 11. Extra flow disruption on the suction side of the blade has a significant influence on the vortex generation and pressure increment in this region. The highest coefficient on the suction side of a low-pressure turbine occurs at $X^* = 0.072$ for clean inflow conditions $(C_p = -0.03)$, while it is moved to $X^* = 0.038$ with the maximum value of $C_p = 0.35$ for $\varphi = 0.91$. This means that the maximum pressure coefficient on the separated flow region of the vibrating blade has been increased by 108%.

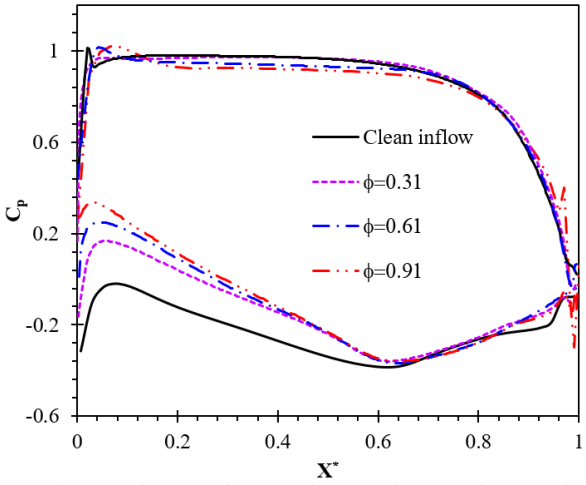

Figure 12. The effects of the inflow disturbance on the instantaneous and time-averaged variations of C_p over the low-pressure turbine surface.

Due to the harmonic motion of the blade, the pressure distributions over the surfaces of the LPT blade fluctuate within a cycle of the oscillation of the blade. The unsteady pressure distributions over the oscillating LPT blade can be divided into a mean value and an amplitude as $P = \bar{P} + P_A\sin(\omega t) + P_B\cos(\omega t)$. In this equation, $\bar{P}$ is the mean value, and P_A and P_B are the coefficients of the Fourier series, respectively. The amplitude of unsteady pressure is calculated as $\sqrt{{P_A}^2 + {P_B}^2}$. No experimental data for the unsteady component of the pressure is available. The coefficient of unsteady pressure amplitude, described as Cp1, normalised by the dynamic inlet pressure, is plotted in Figure 13. It is shown that the unsteady variation of the pressure is affected by the inflow wakes on both surfaces of the LPT blade as the Cp1 distribution shrinks as the frequency of the inflow wakes is increased. The variation of Cp1 between the suction surface and the pressure surface of the oscillating blade subject to a clean inflow is 1.2, whereas 1, 0.9, and 0.7 are recorded at the wake frequencies of 0.31, 0.61, and 0.91, respectively. This is related to the generation of vorticity from the surfaces of the blade. The introduction of the wakes and unsteadiness adds more strength to the generation of the vortex structures over both surfaces of the LPT blade. However, the unsteady vortex structures are generated mainly on the suction surface when no inflow wakes are considered.

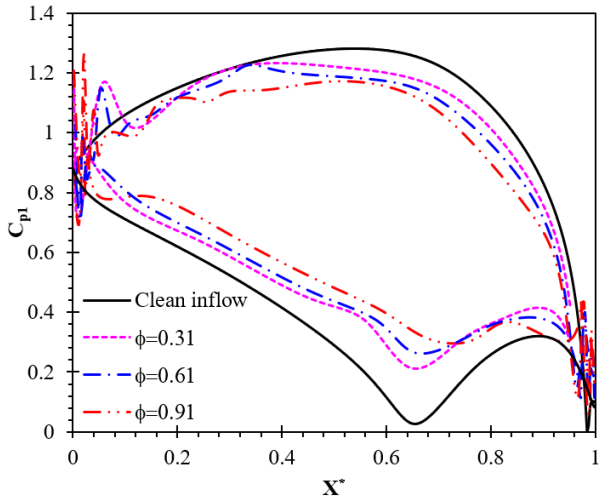

Figure 13. The effects of the inflow disturbance on the unsteady pressure coefficients over the T106 blade.

Figure 14 shows the effects of low-pressure turbine oscillations and inflow disturbances on the time-averaged velocity profiles and turbulent characteristics in the separated area of the blades. It is provided at X/C = 0.95 in the normal direction to the blade surface and close to the trailing edge. It can be seen that the flow separation is influenced by the oscillations, and strong reverse flows are observed for the flexible low-pressure turbine blade with $\phi = 0.31$. It can be seen that the velocity fluctuations become larger by raising the inflow disturbance. Additional turbulence fluctuations are detected close to the blade trailing edge with a higher inflow wake. The peak fluctuation of $u'u'$ is around 0.0092 in the separated region of the rigid blades, while this peak value is 0.0384 in the oscillating blade case with an identical inflow disturbance of $\phi = 0.91$. The maximum fluctuation is 4.17 times larger than the oscillating LPT blade with the same inflow wake.

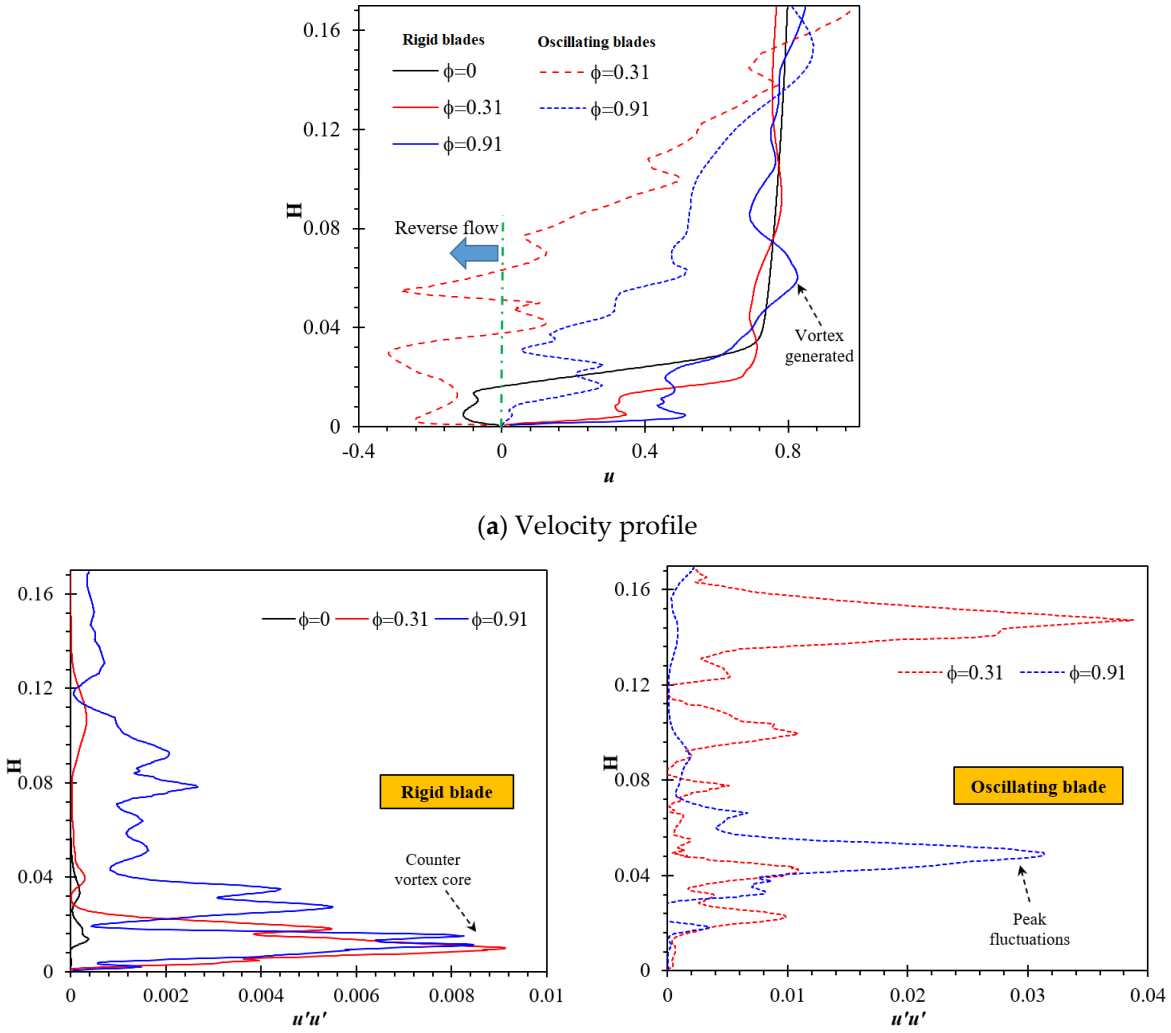

(**a**) Velocity profile

(**b**) Turbulent fluctuations

Figure 14. The effects of the blades oscillations on the velocity and the turbulent fluctuations profiles.

To better compare the velocity fluctuations over the surface of the stationary and oscillating low-pressure T106 turbine blade, a fast Fourier transform (FFT) is performed on the velocity signals on the surface of the blade. The energy spectrum variations with the turbulent frequency are shown in Figure 15. It is observed that due to the oscillations, a stronger energy spectrum is detected at f_{red} = 0.51 and A = 1% C. The results agree with the previous physical discussions. The highest peak of the energy spectrum over the surface of the vibrating blade is detected at F^* = 0.50, which agrees well with the reduced harmonic vibration frequency of the low-pressure turbine blades. Moreover, it is observed

that for both stationary and vibrating turbine blades, the energy spectrum drops below the "−5/3 slope" line, indicating the convergence of simulations.

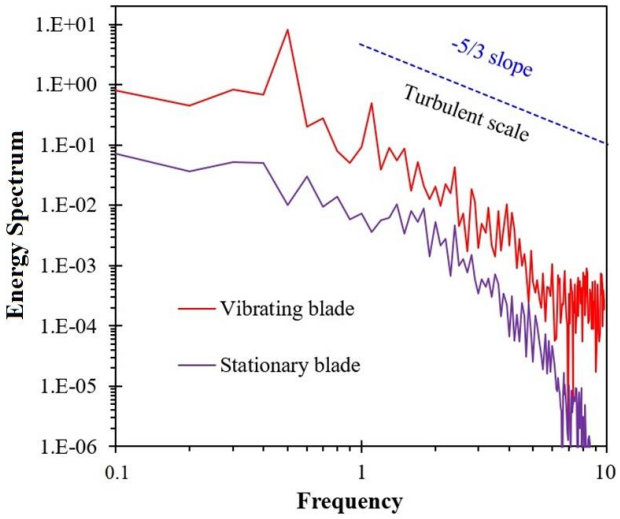

Figure 15. Illustration of the turbulence energy spectrum with and without the blade vibration at Re = 5.18 × 10^4 and φ = 0, at *X*/*C* = 0.7.

5. Discussion

A high-order spectral-hp element DNS method is proposed to extensively analyze the transient flow inside a modern LTP cascade, taking into consideration inflow wakes and blade structure oscillation. The accuracy of the proposed DNS method is validated against an experiment and reference simulations before applying it to further analyzes involving inflow wakes and blade oscillation. The validations in terms of pressure coefficient and wake profile prove that the proposed method can precisely predict the required aerodynamic parameters. In addition, the employed DNS model sufficiently captures high-resolution unsteady flow details, which have been difficult or impossible to achieve with experiments or lower-fidelity methods. It is also revealed that the proposed spectral-hp element DNS method is computationally much more efficient than other conventional finite volume methods.

This study clearly highlights the impact of the blade structure vibration on the evolution of flow structures and the unsteady flow behavior in comparison to the stationary blade based on clean inflow and inflow wakes. When the blade is not oscillating, boundary layer separation typically occurs on the suction surface in the aft region of the blade near the trailing edge, with KH vortex shedding in the wake region. High distortion in the unsteady flow and the vorticity development are detected when the wakes are introduced in the upstream region of the blade, which influences the boundary layer separation and the vortex generation depending on the level of intensity of the wake. The impact is more pronounced on the pressure surface at φ = 0.31 and the suction surface at φ = 0.61, whereas both the pressure and suction surfaces are highly affected by the wakes at φ = 0.91. It is distinctly observed that the oscillation of the blade introduces additional flow disturbances, which, consequently, deform vortex shedding and add more turbulence to the downstream flow. As a result, the maximum TKE is found on the suction surface and the downstream wake region of the oscillating blade.

This observation and understanding of the mechanism of the evolution of vortex structures and the physics behind the interaction between unsteady inflows and oscillating blades are very important for the design and analysis of not just LPTs but also other turbines for energy conversion systems such as wind turbines. For instance, an offshore wind farm consists of multiple large-scale wind turbines, and it is expected that the blades of offshore wind turbines will simultaneously undergo vibration due to their extremely long length and slenderness, and unsteady incoming flows due to the turbulence and wakes from

neighboring wind turbines. The proposed DNS method can explicitly resolve necessary unsteady flow structures and makes it possible to visualize the behavior of the unsteady flow and the vorticity development around turbine blades subject to different sources of flow unsteadiness, such as inflow wakes and blade oscillations.

6. Conclusions

A high-fidelity DNS model is employed to analyze the unsteady behavior inside a T106A low-pressure turbine subject to inflow wakes and blade vibrations. The effect of the unsteadiness due to inflow disturbance and blade oscillation on unsteady flow parameters is investigated. In this paper, for the first time, a DNS method is employed to analyze the flow over a low-pressure turbine blade, taking into account both inflow wakes and blade vibration. The main findings of this study are as follows:

- The flow separation is majorly affected by inflow disturbance and blade vibration. The maximum pressure coefficient on the LP turbine occurs at $X^* = 0.072$ for clean inflow conditions $(C_p = -0.03)$, while it is moved to $X^* = 0.038$ with the maximum value of $C_p = 0.35$ for $\varphi = 0.91$. This means that the maximum pressure coefficient on the separated flow region of the vibrating blade has been increased by 108%.
- The evaluation process of vorticity over the blade surfaces and in the downstream region changes significantly with the level of intensity of the inflow wakes. The blade vibration further intensifies the vortex generation process by imposing more disturbances to the flow and the downstream vortex shedding. The vortex generation and shedding are much greater in comparison with the stationary blade subject to inflow wakes.
- By increasing the inflow disturbance, the separated bubbles tend to shrink, which has a noticeable influence on the pressure value in the downstream region. The inflow disturbance reduces the boundary-layer separation region. It is observed that the highest value of the wake happens at $Y^* = 0.401$ and it moves downward to $Y^* = 0.492$ by raising φ from 0 to 0.91.
- Significant fluctuations are observed in the wake profiles under blade vibration, while the inflow wakes are causing the shift in the peak location of the profile. The maximum wake loss value is reduced by 16.4% by increasing the inflow wake (φ) from 0.31 to 0.91. The vortex structures are broken into smaller pieces in the wake region due to inflow wakes, which results in a shifting of the peak value of the wake loss.

In addition to LPTs, the findings from this paper are also useful for the design and analysis of other turbomachines which can potentially experience aeroelastic instabilities such as offshore wind turbines due to their extremely long blades and the influences of wake and turbulence from neighboring turbines.

Author Contributions: M.E.N.: Conceptualization, Software, Formal analysis, Visualization, Writing—original draft. S.W.N.: Conceptualization, Methodology, Writing—original draft. M.R.: Conceptualization, Writing—review & editing, Funding acquisition, Supervision. All authors have read and agreed to the published version of the manuscript.

Funding: This research was funded by Engineering Physics and Science Research Council of the UK (EPSRC EP/R010633/1).

Conflicts of Interest: The authors declare no conflict of interest.

References

1. Hodson, H.P.; Howell, R.J. The role of transition in high-lift low-pressure turbines for aeroengines. *Prog. Aerosp. Sci.* **2005**, *41*, 419–454. [CrossRef]
2. Jeong, H.; Song, S.J. Surface roughness impact on boundary layer transition and loss mechanisms over a flat-plate under a low-pressure turbine pressure gradient. *J. Turbomach.* **2022**, *144*, 011005. [CrossRef]
3. Butler, R.J.; Byerley, A.R.; VanTreuren, K.; Baughn, J.W. The effect of turbulence intensity and length scale on low-pressure turbine blade aerodynamics. *Int. J. Heat Fluid Flow* **2001**, *22*, 123–133. [CrossRef]

4. Kubacki, S.; Jonak, P.; Dick, E. Evaluation of an algebraic model for laminar-to-turbulent transition on secondary flow loss in a low-pressure turbine cascade with an endwall. *Int. J. Heat Fluid Flow* **2019**, *77*, 98–112. [CrossRef]
5. Han, W.; Zhang, Y.; Li, H.; Yao, M.; Wang, Y.; Feng, Z.; Zhou, D.; Dan, G. Aerodynamic design of the high pressure and low pressure axial turbines for the improved coal-fired recompression SCO_2 reheated Brayton cycle. *Energy* **2019**, *179*, 442–453. [CrossRef]
6. Marty, J. Numerical investigations of separation-induced transition on high-lift low-pressure turbine using RANS and LES methods. *Proc. Inst. Mech. Eng. Part A J. Power Energy* **2014**, *228*, 924–952. [CrossRef]
7. Rahmati, M.; He, L.; Li, Y. The blade profile orientations effects on the aeromechanics of multirow turbomachines. *J. Eng. Gas Turbines Power* **2016**, *138*, 062606. [CrossRef]
8. Rahmati, M.; He, L.; Wang, D.; Li, Y.; Wells, R.; Krishnababu, S. Nonlinear time and frequency domain methods for multirow aeromechanical analysis. *J. Turbomach.* **2014**, *136*, 041010. [CrossRef]
9. Awada, A.; Younes, R.; Ilinca, A. Review of vibration control methods for wind turbines. *Energies* **2021**, *14*, 3058. [CrossRef]
10. Pynaert, N.; Haas, T.; Wauters, J.; Crevecoeur, G.; Degroote, J. Wing Deformation of an Airborne Wind Energy System in Crosswind Flight Using High-Fidelity Fluid–Structure Interaction. *Energies* **2023**, *16*, 602. [CrossRef]
11. Santo, G.; Peeters, M.; Van Paepegem, W.; Degroote, J. Fluid–structure interaction simulations of a wind gust impacting on the blades of a large horizontal axis wind turbine. *Energies* **2020**, *13*, 509. [CrossRef]
12. Naung, S.W.; Rahmati, M.; Farokhi, H. Direct numerical simulation of interaction between transient flow and blade structure in a modern low-pressure turbine. *Int. J. Mech. Sci.* **2021**, *192*, 106104. [CrossRef]
13. Fan, X.; Wang, Y.; Tan, W. Aerodynamic wake oscillator for modeling flow-induced vibration of tandem cylinders with short spans. *Int. J. Mech. Sci.* **2021**, *204*, 106548. [CrossRef]
14. Wang, X.; Zou, Z. Uncertainty analysis of impact of geometric variations on turbine blade performance. *Energy* **2019**, *176*, 67–80. [CrossRef]
15. Zhang, Z.; Santoni, C.; Herges, T.; Sotiropoulos, F.; Khosronejad, A. Time-averaged wind turbine wake flow field prediction using autoencoder convolutional neural networks. *Energies* **2022**, *15*, 41. [CrossRef]
16. Qu, X.; Zhang, Y.; Lu, X.; Lei, Z.; Zhu, J. Effect of periodic wakes and a contoured endwall on secondary flow in a high-lift low-pressure turbine cascade at low Reynolds numbers. *Comput. Fluids* **2019**, *190*, 1–14. [CrossRef]
17. Tucker, P. Computation of unsteady turbomachinery flows: Part 1—Progress and challenges. *Prog. Aerosp. Sci.* **2011**, *47*, 522–545. [CrossRef]
18. Nakhchi, M.; Naung, S.W.; Rahmati, M. Influence of blade vibrations on aerodynamic performance of axial compressor in gas turbine: Direct numerical simulation. *Energy* **2022**, *242*, 122988. [CrossRef]
19. Wang, Y.; Chen, F.; Liu, H.; Chen, H. Large eddy simulation of unsteady transitional flow on the low-pressure turbine blade. *Sci. China Technol. Sci.* **2014**, *57*, 1761–1768. [CrossRef]
20. Siddiqui, M.S.; Fonn, E.; Kvamsdal, T.; Rasheed, A. Finite-volume high-fidelity simulation combined with finite-element-based reduced-order modeling of incompressible flow problems. *Energies* **2019**, *12*, 1271. [CrossRef]
21. Jia, F.; Wang, Z.; Bhaskaran, R.; Paliath, U.; Laskowski, G.M. Accuracy, efficiency and scalability of explicit and implicit FR/CPR schemes in large eddy simulation. *Comput. Fluids* **2019**, *195*, 104316. [CrossRef]
22. Zaki, T.; Wissink, J.; Durbin, P.; Rodi, W. Direct computations of boundary layers distorted by migrating wakes in a linear compressor cascade. *Flow Turbul. Combust.* **2009**, *83*, 307–322. [CrossRef]
23. Wheeler, A.P.; Sandberg, R.D.; Sandham, N.D.; Pichler, R.; Michelassi, V.; Laskowski, G. Direct numerical simulations of a high-pressure turbine vane. *J. Turbomach.* **2016**, *138*, 071003. [CrossRef]
24. Moriguchi, S.; Miyazawa, H.; Furusawa, T.; Yamamoto, S. Large eddy simulation of a linear turbine cascade with a trailing edge cutback. *Energy* **2021**, *220*, 119694. [CrossRef]
25. Iyer, A.; Abe, Y.; Vermeire, B.; Bechlars, P.; Baier, R.; Jameson, A.; Witherden, F.; Vincent, P. High-order accurate direct numerical simulation of flow over a MTU-T161 low pressure turbine blade. *Comput. Fluids* **2021**, *226*, 104989. [CrossRef]
26. Wei, Z.; Ni, M.; Gan, X.; Chen, W.; Chen, P. Generation of unsteady incoming wakes for wake/blade interaction. *Aerosp. Sci. Technol.* **2020**, *106*, 106127. [CrossRef]
27. Moxey, D.; Cantwell, C.D.; Bao, Y.; Cassinelli, A.; Castiglioni, G.; Chun, S.; Juda, E.; Kazemi, E.; Lackhove, K.; Marcon, J. Nektar++: Enhancing the capability and application of high-fidelity spectral/hp element methods. *Comput. Phys. Commun.* **2020**, *249*, 107110. [CrossRef]
28. Cantwell, C.D.; Moxey, D.; Comerford, A.; Bolis, A.; Rocco, G.; Mengaldo, G.; De Grazia, D.; Yakovlev, S.; Lombard, J.-E.; Ekelschot, D. Nektar++: An open-source spectral/hp element framework. *Comput. Phys. Commun.* **2015**, *192*, 205–219. [CrossRef]
29. Bao, Y.; Palacios, R.; Graham, M.; Sherwin, S. Generalized thick strip modelling for vortex-induced vibration of long flexible cylinders. *J. Comput. Phys.* **2016**, *321*, 1079–1097. [CrossRef]
30. Cassinelli, A.; Adami, P.; Montomoli, F.; Sherwin, S.J. On the effect of wake passing on a low pressure turbine cascade using spectral/*hp* element methods. *Bull. Am. Phys. Soc.* **2019**, *64*, 13.
31. Yan, Z.-G.; Pan, Y.; Castiglioni, G.; Hillewaert, K.; Peiró, J.; Moxey, D.; Sherwin, S.J. Nektar++: Design and implementation of an implicit, spectral/hp element, compressible flow solver using a Jacobian-free Newton Krylov approach. *Comput. Math. Appl.* **2021**, *81*, 351–372. [CrossRef]

32. Nakhchi, M.; Rahmati, M. Direct numerical simulations of flutter instabilities over a vibrating turbine blade cascade. *J. Fluids Struct.* **2021**, *104*, 103324. [CrossRef]
33. Michelassi, V.; Chen, L.-W.; Pichler, R.; Sandberg, R.D. Compressible Direct Numerical Simulation of Low-Pressure Turbines—Part II: Effect of Inflow Disturbances. *J. Turbomach.* **2015**, *137*, 071005. [CrossRef]
34. Stadtmüller, P. *Investigation of Wake-Induced Transition on the LP Turbine Cascade T106A-EIZ. DFG-Verbundproject Fo 136/11*; Universität der Bundeswehr München: Neubiberg, Germany, 2001.
35. Vos, P.E.; Sherwin, S.J.; Kirby, R.M. From h to p efficiently: Implementing finite and spectral/hp element methods to achieve optimal performance for low-and high-order discretisations. *J. Comput. Phys.* **2010**, *229*, 5161–5181. [CrossRef]
36. Nakhchi, M.; Naung, S.W.; Rahmati, M. High-resolution direct numerical simulations of flow structure and aerodynamic performance of wind turbine airfoil at wide range of Reynolds numbers. *Energy* **2021**, *225*, 120261. [CrossRef]
37. Dong, S.; Karniadakis, G.E.; Chryssostomidis, C. A robust and accurate outflow boundary condition for incompressible flow simulations on severely-truncated unbounded domains. *J. Comput. Phys.* **2014**, *261*, 83–105. [CrossRef]
38. Cassinelli, A.; Xu, H.; Montomoli, F.; Adami, P.; Vazquez Diaz, R.; Sherwin, S.J. On the Effect of Inflow Disturbances on the Flow Past a Linear LPT Vane Using Spectral/hp Element Methods. In Proceedings of the ASME Turbo Expo 2019: Turbomachinery Technical Conference and Exposition, Arizona, PX, USA, 17–21 June 2019; p. V02CT41A032.
39. Stadtmüller, P.; Fottner, L. A Test Case for the Numerical Investigation of Wake Passing Effects on a Highly Loaded LP Turbine Cascade Blade. In Proceedings of the ASME Turbo Expo 2001: Power for Land, Sea, and Air, New Orleans, LA, USA, 4–7 June 2001; American Society of Mechanical Engineers: New York, NY, USA, 2001; p. V001T03A015.
40. Nakhchi, M.E.; Naung, S.W.; Rahmati, M. DNS of secondary flows over oscillating low-pressure turbine using spectral/hp element method. *Int. J. Heat Fluid Flow* **2020**, *86*, 108684. [CrossRef]
41. Sieverding, C.H.; Ottolia, D.; Bagnera, C.; Comadoro, A.; Brouckaert, J.-F.; Desse, J.-M. Unsteady turbine blade wake characteristics. *J. Turbomach.* **2004**, *126*, 551–559. [CrossRef]